A computational investigation of Orbital Overlap versus Energy Degeneracy Covalency in $[UE_2]^{2+}$ (E = O, S, Se, Te) complexes

James A. Platts*[a] and Robert J. Baker[b]

[a] School of Chemistry, Cardiff University, Park Place, Cardiff CF10 3AT, UK.

[b] School of Chemistry, University of Dublin, Trinity College, Dublin 2, Ireland.

* Author for correspondence

Email: platts@cardiff.ac.uk

Phone: +44-2920-874950

ABSTRACT

The extent and nature of covalency in actinide complexes is an important and complex question. There are two main mechanism of covalency, namely overlap of orbitals or degeneracy of the energies of the ligand and actinide metal, and computational approaches can play a significant part in rationalising the relative importance of each. In this work we use a suite of computational approaches including Natural Bond Orbitals (NBO), Quantum Theory of Atoms in Molecules (QTAIM) and Interacting Quantum Atoms (IQA) to probe these effects in $[E=U=E]^{2+}$ (E = O, S, Se, Te) and $[UE_2(H_2O)_5]^{2+}$ compounds. All methods indicate increased bond order and reduced charge separation on descending the group. Donation from filled n*p* orbitals on E into formally empty orbitals on U is evident, with 5*f* and 6*d* orbitals the most populated. NBO analysis quantifies orbital interactions, finding energy separation is largest for E = O, while for E = Te the atomic orbitals are almost degenerate. However, NBO and IQA data suggests that although overlap is greater for heavier chalcogens, stabilisation due to covalency is greatest for E = O. Thus, for the heavier chalcogens we find that covalency is driven by near-degeneracy of orbitals involved, which does not stabilise the complexes to the same extent as overlap-driven covalency in uranyl. In the hydrated ions the same trends are broadly reproduced, albeit with more stabilisation and a lower HOMO-LUMO gap. The structure and stability of the $[O=U=S]^{2+}$ ion is also examined, showing evidence for an inverse trans-influence. Finally bending of the $[US_2(H_2O)_5]^{2+}$ ion has been examined, suggesting a possible meta-stable *cis*-form.

INTRODUCTION

Bonding between atoms is a fundamental concept in science and the role of s-, p- and d-orbitals in bonding is sufficiently well developed so that current theories can rationalise structure and reactivity trends in the overwhelming majority of cases for s,- p- and d-block chemistry.[1] However, the situation is much less clear-cut when the f-orbitals are involved and the idea of covalency in actinide (5f) complexes is an enduring point of contention in the literature. The concept of 5f-orbitals involvement in covalent bonding can be traced to Seaborg's justification for the separation of Am,[2] and has since been evoked by numerous authors to understand the bonding in a broad range of compounds. For example, the organometallic actinideocenes $[(COT)_2An]$ (An = Th - Pu)[3] have proven to be fertile ground for discriminating 5f and 6d bonding contributions, and the situation for all actinidocenes, except Th, is more complex than first thought and accepted as multiconfigurational.[4] A second illustrative example was the interpretation of the CO stretching frequency in the IR spectrum of the complex $[Cp'_3U(CO)]$ ($Cp' = C_5H_4SiMe_3$) as a result of 5f-π* overlap, analogous to transition metal carbonyl complexes.[5] Changing the Cp′ ligand to Cp* or C_5Me_4H revealed a pronounced effect on the ν(CO);[6] computational studies showed no symmetry matching 5f-orbitals on U, and the effect was traced to overlap of ligand orbitals with the CO π* orbital.[7] This was corroborated by experimental and theoretical investigations of the analogous $[Cp^*_3Th(CO)]$.[8] These simple organometallic examples highlight the complex nature of actinide species, and that multiple probes are required to fully understand the bonding.

Despite the well held and supported assumption that ionic bonding is important,[9] more recent work[10] has built upon older computational studies[9] that show that the f-orbitals may not be the major contribution to bonding and the 6d are a more appropriate description. Taken globally, a study of the chemistry of the actinides have produced molecules that challenge established ideas of chemical bonding and covalency. From these studies, two models of covalent bonding have been established: orbital overlap and energy degeneracy driven covalency.[11] In a molecular orbital description, the mixing parameter λ (Equation 1) indicates the extent of covalency, where H_{ML} is the Hamiltonian matrix element between orbitals and ΔE_{ML} is the energy difference between them.

$$\lambda = \frac{H_{ML}}{\Delta E_{ML}} \qquad (1)$$

It therefore follows that there are two means to achieve large λ: large H_{ML} (*i.e.* orbital overlap covalency, involving mixing of MOs of ligand and metal) or small ΔE_{ML} (*i.e.* energy near

degeneracy). Numerous spectroscopic techniques can be used to probe covalency, with X-ray Absorption Spectroscopy (XAS) at the forefront. Whilst this gives insight into 5f [12] or 6d [13] metal or ligand based[14] orbital contributions to bonding,[15] it is not able to clearly differentiate the two. However, it should be noted that XAS experiments are challenging and analysis difficult. Computational chemistry allows bonding to be analysed and significant strides have been taken in recent years, and combined approaches have clarified ideas of covalency in actinides.[16] Thus proposed that, in general, early actinides have a large H_{ML} contribution whilst later actinides have a small ΔE_{ML}, due to the increasing core-like character of the 5f orbitals in the later actinides. This has applications in Ln/An separation for next generation fuel cycles.[17]

One important instance of d- and f-orbital overlap with ligand p-orbitals is in a conventional orbital overlap description of covalency in the uranyl ion $[UO_2]^{2+}$.[18] Most importantly, the 'semi-core' 6p orbital is invoked in bonding, which destabilises the σ orbitals relative to the π orbitals, and is termed 'pushing from below'.[19] The experimental justification for invoking 6p as well as 5f and 6d molecular orbitals has been presented by Denning in a series of seminal works[20] and has been interrogated computationally by several authors using a variety of methods and metrics.[9] A qualitative molecular orbital diagram (Figure 1) can be derived which explains spectroscopic and structural properties, not only of uranyl(VI) but also of actinyl(V) and (VI) ions (actinyl = U, Np, Pu, Am). Missing from this diagram are spin-orbit splittings which become more relevant for the heavier actinides, but for UO_2 are of the order of 1 eV.[21] Moreover, overlap with f-orbitals imparts the uranyl ion linear geometry, as compared to d-block complexes such as $[MoO_2]^{2+}$, which are typically *cis*. This has recently been proposed to be a manifestation of the inverse trans influence (ITI), stemming from the involvement of the 6p orbital, that is now noted in uranium compounds in variable oxidation states and with non-oxo ligands.[22] The equatorial coordination sphere of uranyl can include 4-6 ligands which are mainly ionic in their bonding, though in certain cases these ligands can form covalent interactions that may be observed spectroscopically.[23]

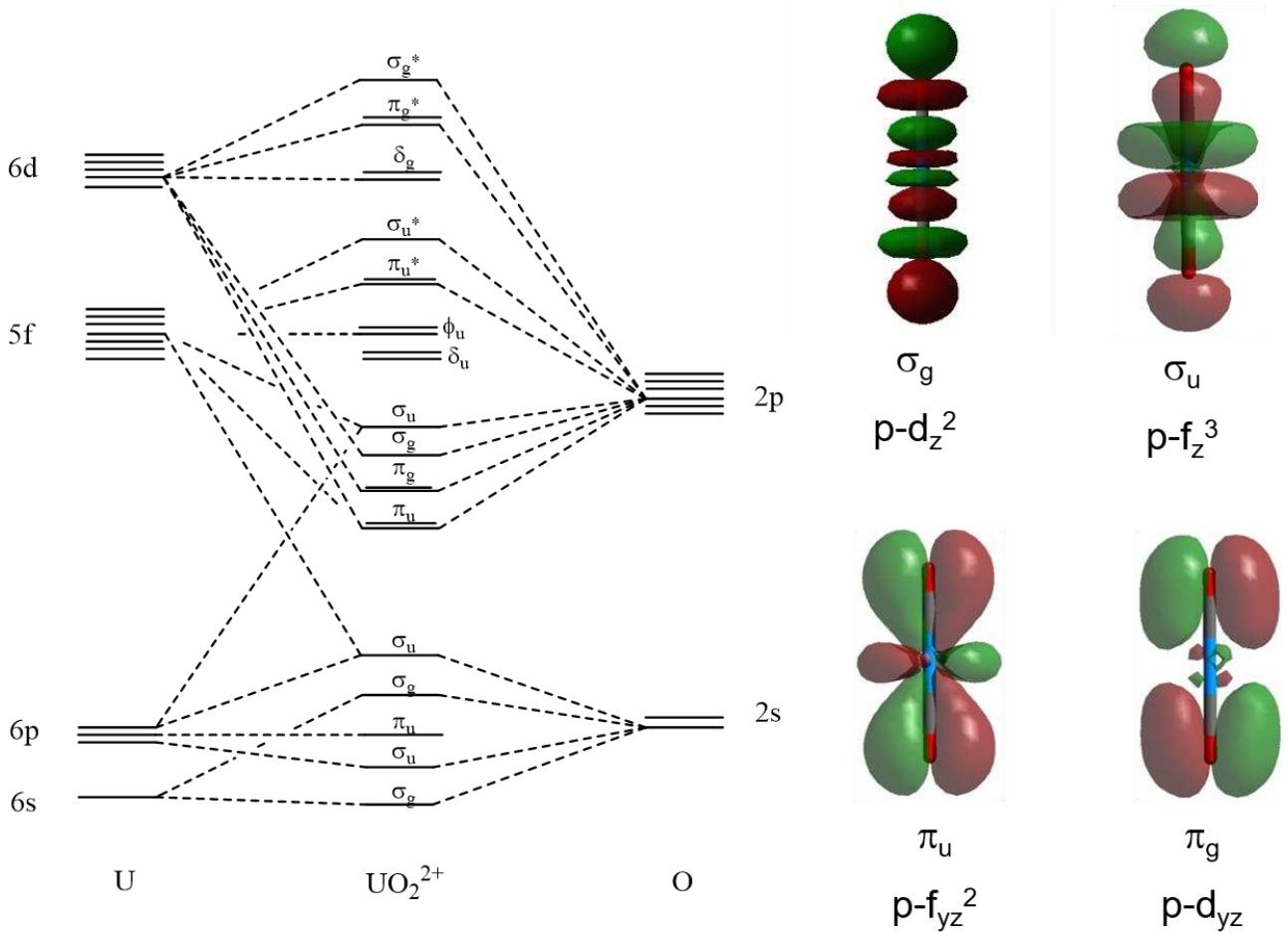

Figure 1. Qualitative MO diagram for bonding in the uranyl ion along with canonical representations of the orbital overlap.

Striking by their absence are experimentally characterised heavier analogues of the uranyl ion $[UE_2]^{2+}$ (E = S, Se, Te). Indeed, only one report features the $[US_2]^{2+}$ ion from a mass spectrometry study,[24] although $[OUE]^{2+}$ (E = S, Se)[25] and a related carbene[26] $[OUCR_2]^{2+}$ have been stabilised. Computational chemistry can be used to elucidate bonding in the series: the conventional model of orbital overlap covalency is well established for the uranyl ion (*vide supra*), but as the radial extent of the *n*p orbitals of heavier congeners increases, orbital overlap and near energy driven covalency may combine or even cross over. In this report we detail a multi-metric approach to probe covalency in the bare $D_{\infty h}$ $[UE_2]^{2+}$ ions and, to provide more realistic experimental targets, we also examine the hydrated species $[UE_2(H_2O)_5]^{2+}$. We note that theoretical studies suggest a triangular di-hapto U…S_2 isomer is lower in energy than the linear thiouranyl form,[24,27] with significant multi-reference character in the triplet ground state. Since our goal here is to explore the bonding in model compounds rather than to explore potential energy surfaces in detail, we concentrate mainly on the closed-shell linear uranyl analogues, with the aim of applying similar analysis to experimentally observed structures in future publications.

EXPERIMENTAL

Computational Methods

All geometry optimisations were performed using the PBE0 functional[28] with Stuttgart 1997 60e core/basis on U[29] and def2-TZVP[30] on E using Gaussian09.[31] The basis set on chalcogens includes all electrons explicitly for O, S and Se but introduces a 28-electron core potential for Te to account for scalar relativistic effects. We note that this method was recently shown to yield electron density and derived properties in close agreement with CASSCF methods.[22a] All structures were confirmed as minima *via* harmonic frequency calculations. Natural bond orbital[32] (NBO) and Atoms in Molecules[33] (QTAIM) analyses were performed using Gaussian09 and AIMAll,[34] respectively. Interacting Quantum Atoms[35] (IQA) data were obtained using a Hartree-Fock wavefunction and the same basis set, since application of this approach to Kohn-Sham orbitals is not appropriate.

RESULTS AND DISCUSSION

Optimised geometry and details of normal mode vibrations are reported in Table 1: data for uranyl is in good agreement with previous experimental and theoretical reports.[9] Progressively longer U-E bond lengths are observed on descending the group: these changes are larger than can be accounted for by increases in covalent radius of E alone,[36] indicating that changes in the electronic structure of the ions is also present. Vibrational data follows a similar trend: wavenumbers for bend and stretch normal modes fall, as might be expected on the basis of reduced mass, but force constants are also smaller for E = S, Se, Te than they are for O. The reduction in force constant is not monotonic, and values for $[USe_2]^{2+}$ are comparable to those for $[US_2]^{2+}$.

Table 1 Optimised geometry and normal mode vibrations for $[UE_2]^{2+}$ (Å, cm^{-1} and mDyne/Å)

$[UE_2]^{2+}$	r(U-E)	ν(bend) / force constant	ν(symm)	ν(asymm)
O	1.679	179.4 / 0.34	1092.5 / 11.25	1183.7 / 14.85
S	2.177	88.1 / 0.18	528.8 / 5.27	601.7 / 8.35
Se	2.342	50.5 / 0.16	302.0 / 4.29	393.4 / 9.94
Te	2.584	27.8 / 0.08	205.2 / 3.22	298.2 / 8.92

To explore the origin of these changes in more detail, we examined the electronic structure of all four complexes, initially in the form of their canonical molecular orbitals (Figure 2). Visually,

differences are small for E = O, S and Se, but the σ_u HOMO for E = Te is notably more diffuse when plotted at this level. MO energies in Figure 3 reveal a more nuanced picture: absolute energies rise sharply from E = O to S, then more steadily for Se and Te, presumably due to the longer bond lengths and reduced charge on E atom (*vide infra*). The HOMO energy rises more quickly than does that of the LUMO, leading to significant narrowing of the gap between these levels, from 6.1 eV for O to just 2.4 eV for Te. In all cases, HOMO has σ_u and LUMO ϕ_u character, although for E = Se and Te this almost degenerate with the π_u MO. Larger changes are found for the lower-lying occupied orbitals: in particular, HOMO-1 for uranyl is σ_g, but for the heavier chalcogens this orbital lies below the occupied π_u and π_g MOs. A similar pattern is seen for the anti-bonding σ^*_u MO, which is high in energy for E = O but comparatively lower in the other species, and found at similar energies to the σ^*_g and δ_g orbitals. In contrast, the anti-bonding π^*_g and π^*_u MOs are much less affected by the identity of E.

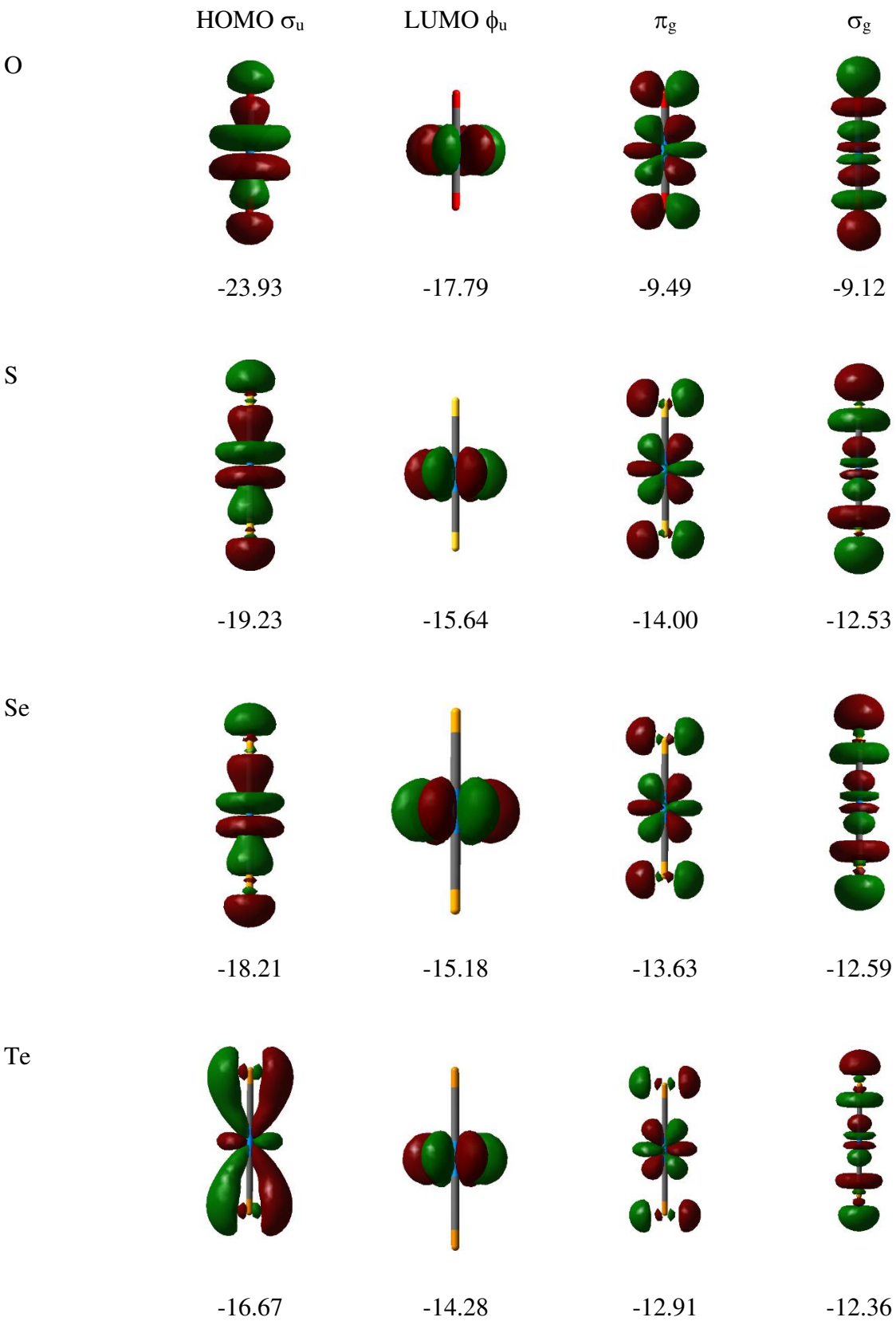

Figure 2 Canonical MOs, plotted at 0.05 probability isosurface level, with MO energy in eV

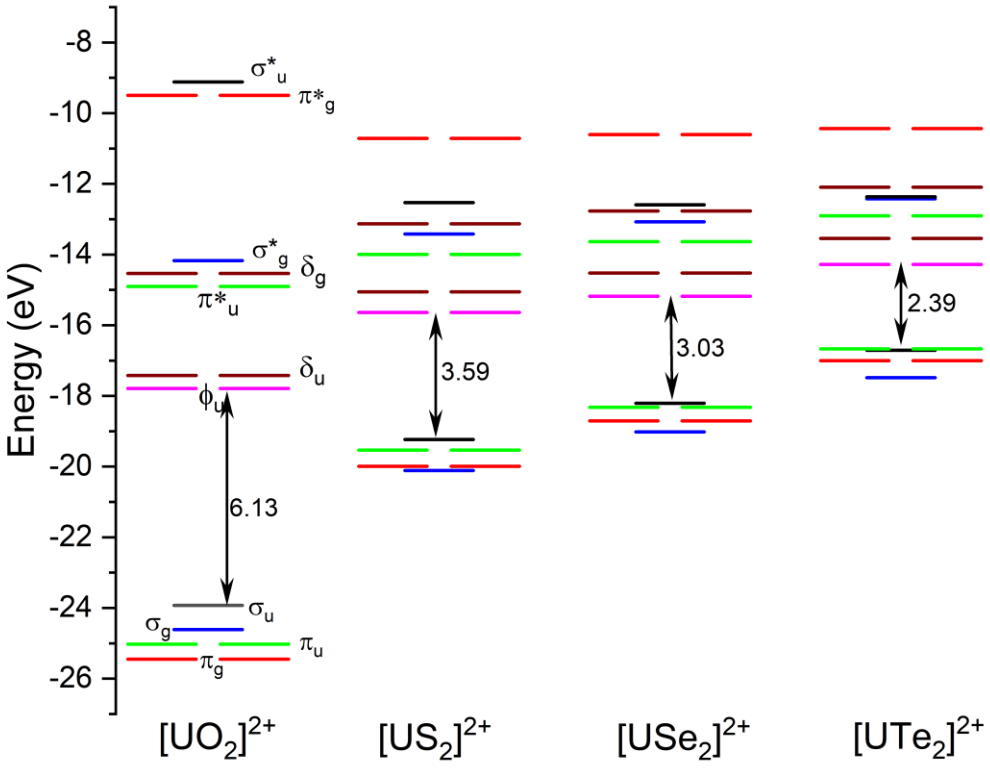

Figure 3 MO energy levels. Colour code – Red: π_g/ π^*_g; Green: π_u/ π^*_u; Blue: σ_g/ σ^*_g; Black: σ_u/ σ^*_u; Pink: φ_u; Brown: δ_u. HOMO-LUMO separation is indicated in eV.

NBO analysis (Table 2) reveals a consistent picture of positively charged U, although in all cases charges are much smaller than the formal values of +6 and -2. Charges are greatest in magnitude for E = O, and progressively fall down the group such that E = Te has a charge of just +1 e on U, such that according to this definition E is positive for S, Se and Te. Natural atomic orbitals and the resulting electron configuration on U sheds more light on origin of these changes. In all cases we find substantial population of 5f and 6d orbitals on U, and that these populations increase down the group. 7s and 7p orbitals are less populated, but this increases for the heavier chalcogens. Donation into the formally empty valence orbitals on U leads to significant covalent character, as determined by the Wiberg bond order. Even for O the bond order is over 2, while for the heavier elements this approaches 3, suggesting greater covalency in the heavier, softer chalcogens reflecting the greater donation into formally empty orbitals on U.

Table 2 NBO charge, configuration and Wiberg bond order data

	q(U)	U config	Wiberg BO
O	2.749	$7s^{0.05}\ 5f^{2.49}\ 6d^{1.06}\ 7p^{0.04}$	2.28
S	1.492	$7s^{0.04}\ 5f^{2.86}\ 6d^{1.64}\ 7p^{0.08}$	2.65
Se	1.325	$7s^{0.07}\ 5f^{2.86}\ 6d^{1.71}\ 7p^{0.09}$	2.68
Te	1.047	$7s^{0.15}\ 5f^{2.88}\ 6d^{1.83}\ 7p^{0.10}$	2.76

NBO analysis offers a means to quantify the contributions to covalency highlighted in Equation 1. In each complex, three bonding NBOs per bond, one with σ- and two with π-character, are present. The former stems from a combination of p_z-orbital on E with d_{z2} and f_0 on U, and the latter $p_{x/y}$ on E with $d_{xz/yz}$ and $f_{\pm1}$ on U. Details of the orbital make up of bonding NBOs is shown in Table 3. Values for E = O are largely as expected for metal-ligand bonds, with low-lying valence orbitals on O donating into higher-lying ones on U, and contributing between two-thirds and three-quarters of the total occupancy of each NBO. For the heavier analogues, the valence orbitals on E are higher lying and those on U lower in energy, such that the energy separation term in Eq. (1) is smaller. The contribution to the NBO from E is reduced, but remains more than 50% in all cases. These trends reach their extreme in the π-bonding orbitals in $[UTe_2]^{2+}$, for which AOs on U and Te of very similar energy make almost equal contributions.

Table 3 Bonding orbitals from NBO analysis

	Occupancy	ε_{NBO} /au	%U	%E	ε_{AO} U [a] /au	ε_{AO} E /au
O σ	1.918	-1.177	33	67	-0.230 / -0.666	-0.852
π	1.988	-0.932	24	76	-0.430 / -0.612	-0.817
S σ	1.882	-0.868	43	57	-0.384 / -0.618	-0.651
π	1.995	-0.729	35	65	-0.472 / -0.570	-0.628
Se σ	1.880	-0.821	43	57	-0.398 / -0.597	-0.605
π	1.996	-0.684	36	64	-0.468 / -0.554	-0.605
Te σ	1.891	-0.716	39	61	-0.315 / -0.561	-0.533
π	1.997	-0.622	45	55	-0.455 / -0.521	-0.541

[a] Energy of individual NAO's involved in each NBP, reported as *d* / *f* for σ- and *p* / *d* for π

NBO also highlights interactions that lie outside the Lewis structure through use of second-order perturbation theory (Table 4). In all cases, the dominant interactions identified correspond to donation from lone pair on E to formally empty orbitals on U: donation into a *sd*-hybrid and an unhybridised *p*-orbital are present, with approximately equal contributions to stabilisation. The strongest such interactions are found for E = O, in which large orbital overlap (H_{ij}) and small energy difference (ΔE_{ij}) combine to yield substantial stabilisation, with donation into the *sd*-hybrid the stronger effect. For E = S, the order of interaction strength is reversed: donation into an empty *p*-orbital on U is stronger despite greater ΔE_{ij}, and is driven by greater overlap, whereas donation into *sd*-hybrid is weakened due to reduced overlap. For E = Se and Te, this trend is further exacerbated: increased orbital energy separation and/or reduced overlap reduces the strength of both types of interaction, most notably for E = Se. This data therefore indicates that a subtle balance of orbital overlap and degeneracy determines covalency in U—E bonds, leading to the overall trend of increased overlap but reduced stabilisation due to covalency on descending the group.

Table 4 Second-order perturbation NBO data

	E(2) / kJ mol^{-1}	ΔE_{ML} / au	H_{ML} / au
O LP → *sd*	99.6	1.35	0.160
LP → *p*	68.4	1.62	0.146
S LP → *sd*	56.2	1.36	0.121
LP → *p*	94.0	2.52	0.213
Se LP → *sd*	47.4	1.60	0.121
LP → *p*	75.6	2.69	0.198
Te LP → *sd*	67.5	1.61	0.145
LP → *p*	46.2	2.55	0.151

QTAIM analysis, in the form of properties evaluated at the U—E bond critical point (Table 5) complements NBO data to reveal a more complex picture. The electron density at the bond critical point (bcp), often taken as a proxy for bond strength, is much larger for E = O than for the other species and falls further from S through Se to Te. The Laplacian of the density, widely used as an indicator of ionic/covalent nature, is large and positive for E = O but close to zero for the other species and slightly negative for E = S. Potential (V) and kinetic (G) energy densities are much larger in magnitude for E = O, leading to a much larger overall energy density, H, but in cases all potential energy dominates to yield a negative overall value. Negative energy density at a bcp is

often interpreted as evidence of covalent bonding, so there is an apparent contradiction between this and $\nabla^2\rho$ that will be addressed in more detail below.

Table 5 QTAIM bond critical point data, atomic charges (au), bond orders and oxidation states[37]

	ρ	$\nabla^2\rho$	V	G	H	q(U)	δ(U,E)	OS(U)
O	0.386	+0.373	-0.947	+0.520	-0.427	3.312	2.28	5.59
S	0.195	-0.033	-0.273	+0.133	-0.140	2.239	2.52	4.67
Se	0.153	+0.018	-0.197	+0.101	-0.096	2.009	2.58	4.59
Te	0.111	+0.054	-0.125	+0.069	-0.056	1.676	2.65	4.33

Integrated atomic charge on U is uniformly positive for all E, and decreases markedly from O to S, then less so for Se and Te. Values are larger than those from NBO analysis, but the trends are very similar. Delocalisation indices, δ(U,E), a QTAIM-based measure of bond order, are in close agreement with NBO values, indicating substantial covalent nature for all U—E bonds: least for E = O, and rising slightly across S, Se and Te. This is quite different from that reported by Brown et al, who found slightly reduced bond order in U-S bond compared to U-O in a series of $[OUE]^{2+}$ (E = O, S, Se) complexes stabilised by equatorial NR_2 ligands,[25] indicating the markedly different electronic structure in these more symmetrical complexes. Kerridge defines a QTAIM metric of oxidation state through the localisation index of the atom in question:[38] our data indicate that U is close to the formal +6 oxidation state for E = O, but that this is reduced to around +4.5 for heavier, softer chalcogens.

A consistent picture of U—E bonding that accounts for NBO and QTAIM data can be constructed for E = S, Se and Te: donation from E into formally empty orbitals on U lead to charges and bond orders that lie between the extremes of fully ionic and fully covalent, while moderate values of ρ and $\nabla^2\rho$ and small negative values of energy density at the bcp are typical of polar covalent bonds. However, the bonding pattern for E = O is less clear from this data: NBO and QTAIM charges and bond orders as well as the Laplacian at the bcp suggest this is the most ionic/least covalent of the species considered, but values of ρ and H at the bcp indicate the opposite. The apparent discrepancy between different density-based measures of bond strength has been noted before for comparisons of uranyl against imido $[HN=U=NH]^{2+}$ and carbene $[H_2C=U=CH_2]^{2+}$ analogues.[22]

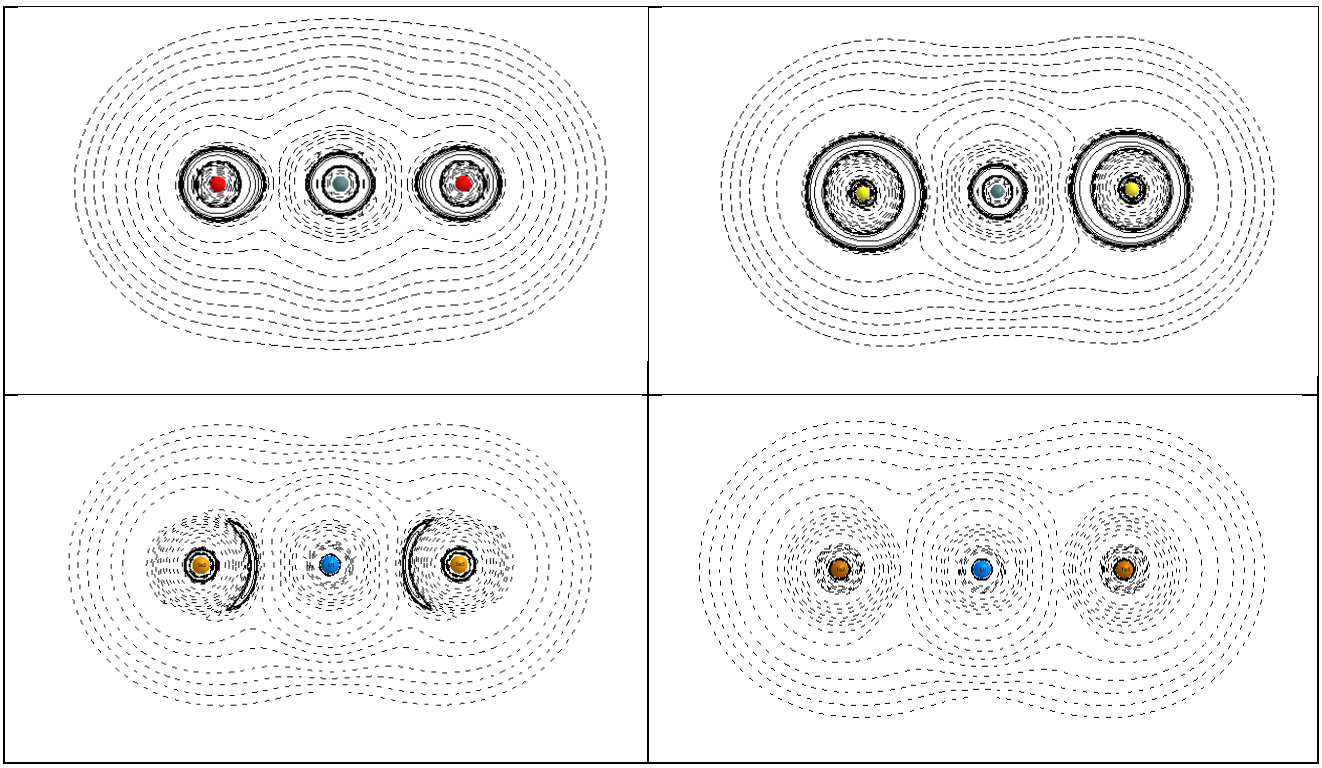

Figure 3 Contour plots of Laplacian, with positive values (charge depletion) shown as dashed lines and negative (charge accumulation) as solid lines: top row E = O and S, bottom row E = Se and Te.

To shed more light on this apparent discrepancy, and on the difference between O and S, we plot a range of properties in the internuclear region. Contour plots of the Laplacian of the electron density (Figure 3) are rather similar between O and S, with large areas of charge depletion separating relatively small islands of accumulation centred on each atom. There is some evidence of polarisation of the density on E atoms towards the positive U centre, a feature that is more apparent for E = O than S. For the heavier analogues, the local charge concentrations shrink: with E = Se a small region of negative Laplacian is found in the internuclear region, whereas in E = Te we find no such concentration, and the Laplacian is positive throughout and only negative in the shell structure very close to the nuclei.

Plots of density and related properties along the bond path for E = O and S are shown in Figure 4. These show very little difference up to approximately 1.5 au from U, after which curves diverge. For E = O, ρ remains large (> 0.3 au) along the whole bond path, while for E = S it falls much further as the bond path extends further from U. The bond critical point (located at r = 1.74 au for O, 2.32 au for S) is, by definition, the point with lowest electron density along the bond direction. For $[UO_2]^{2+}$ this lies within the valence shell of U, and beyond this point ρ rises as the valence shell of O dominates. In contrast, the bond critical point for $[US_2]^{2+}$ lies well outside the valence shell of

U in a relatively flat region of density that separates the shell structures of U and S, a pattern that is much more typical of metal-ligand bonding.

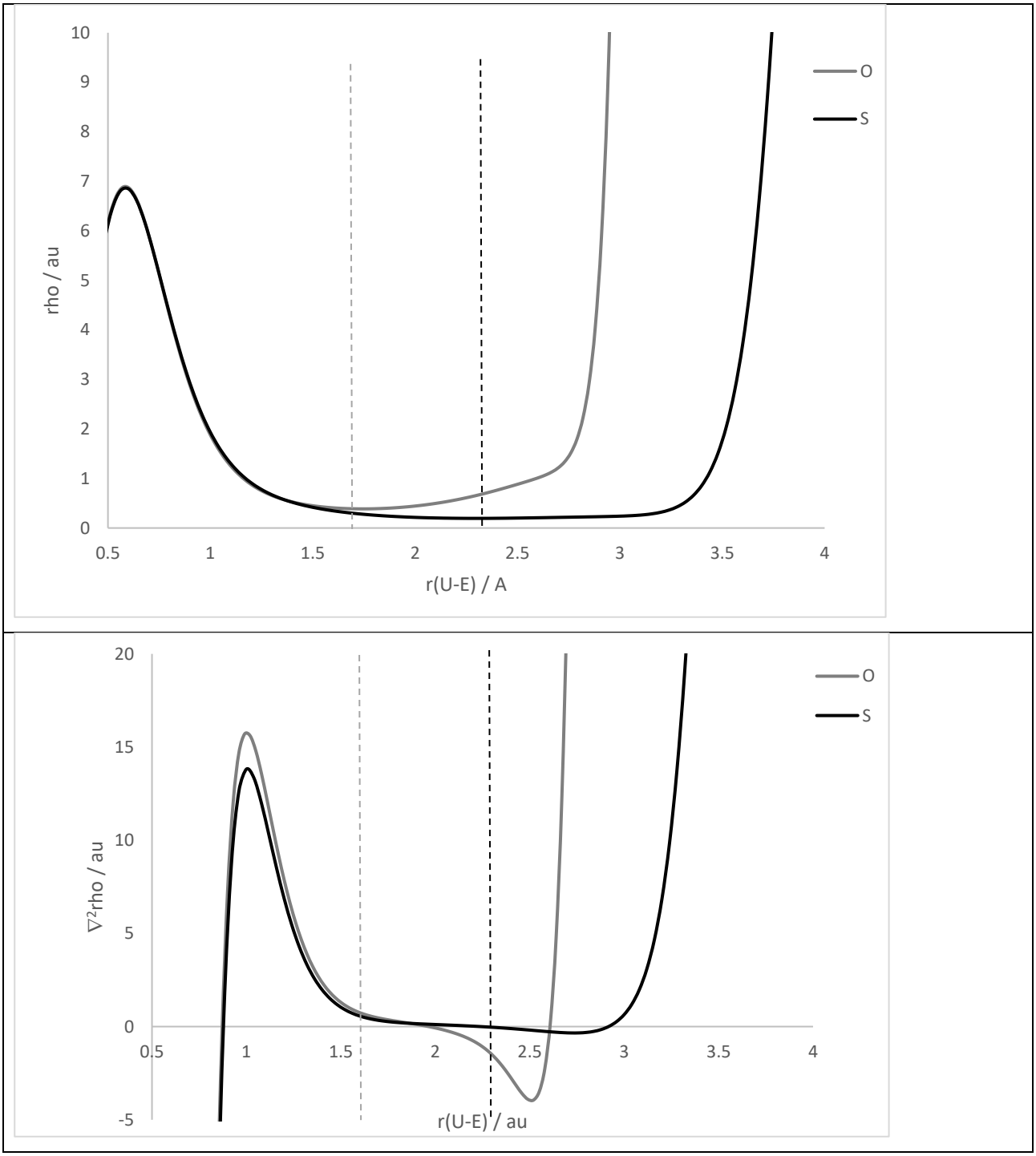

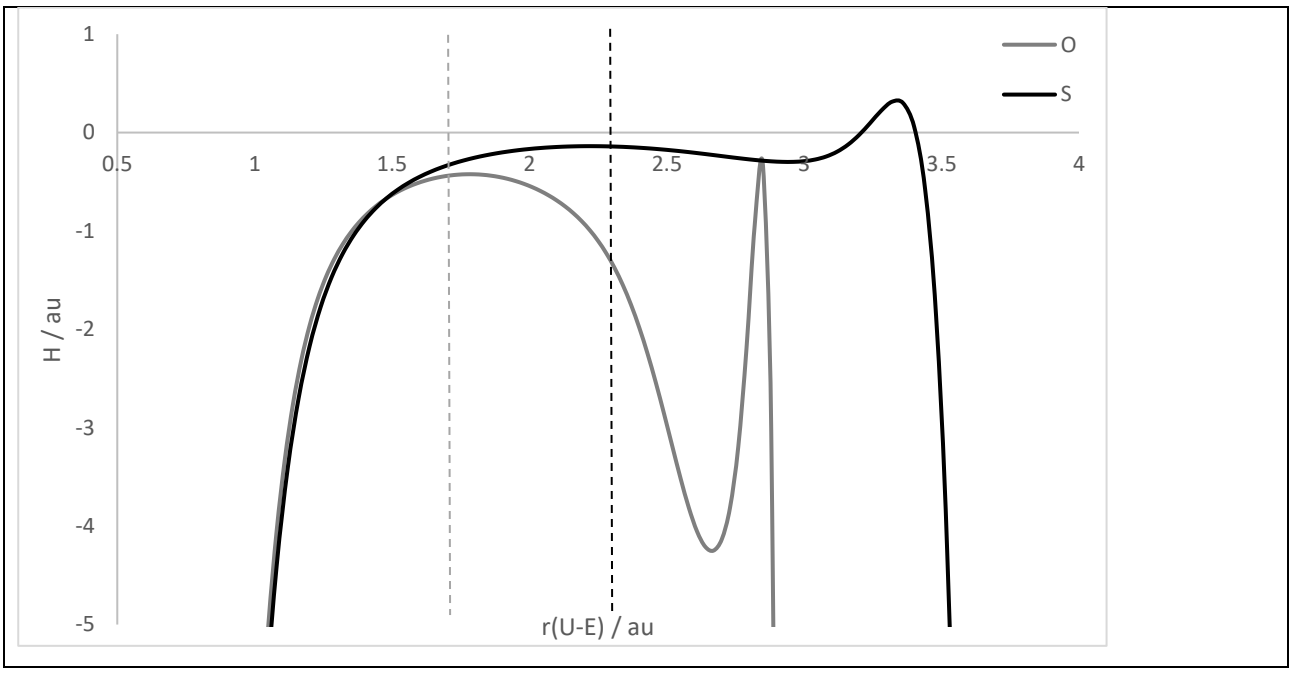

Figure 4 Electron density, Laplacian and energy density in U-E internuclear region, plotted against distance from U. Bond critical points located at 1.74 and 2.32 au from U, respectively, are denoted by dashed lines.

The importance of the shell structure of the atoms involved in U-E bonding is illustrated by plots of the Laplacian and energy density. For E = O, both properties exhibit strong minima around 2.5 au from U: this is due to the inherent shell structure of O itself, rather than to any specific feature of U-O bonding, and represents the valence shell charge concentration (VSCC) present even in isolated atoms.[39] A similar but much reduced feature is also present for E = S, in a similar manner to those for isolated atoms. For E = O the bond critical point lies just outside O's VSCC, in a region where the Laplacian is changing rapidly, just inside the positive region associated with U, and close to the maximum of the (everywhere negative) energy density. Taken together, these plots offer an explanation for the unusual bcp properties found for U-O (*i.e.* high ρ, positive $\nabla^2\rho$ but large, negative H). The U-O bond is very short indeed, due to the cooperative effect of strong ionic *and* covalent bonding, which means that the bcp is found within the valence shell of U, such that the density does not fall to values more typical of metal-ligand bonds. This places the bcp in a region where $\nabla^2\rho$ is rapidly varying, but just inside the positive lobe on U rather than the negative one due to O, and just within the associated negative region of energy density. This indicates the importance of assessing covalency from a rounded picture of multiple properties, rather than solely on a single property such as ρ_{bcp} to quantify this property.

A deeper interrogation of QTAIM properties sheds further light on the difference between E = O and the rest of the series. Atomic multipoles complement atomic charges by determining the distribution of charge within the relevant atomic basin (Table 6). The atomic dipole moment of U is zero by symmetry in all cases, but those of E are oriented along the symmetry axis in a direction reflecting intramolecular polarisation of density towards U, an effect that is much smaller for O than for the larger, softer S, Se and Te. Quadrupole moments on U are not necessarily zero, although the axial symmetry of all species means a single value characterises the traceless tensor. The positive value of Q_{zz} on U for E = O indicates compression of electron density along this axis, such that density is preferentially oriented into the equatorial plane. In contrast, all other members of the series have negative Q_{zz} on U, showing that density is accumulated along the internuclear axis. Q_{zz} on E is uniformly positive, showing that electron density is accumulated into perpendicular axes, an effect that increases from O to Te.

Table 6 QTAIM atomic multipoles and surface virials (au). All values for E are reported for the atom with positive *z*-coordinate.

	O	S	Se	Te
μ_z (E)	+0.367	+0.667	+0.718	+0.809
Q_{zz} (U)	+5.241	-1.493	-3.275	-5.683
Q_{zz} (E)	+1.358	+2.851	+3.132	+3.497
V_s (U|E)	-0.478	-0.189	-0.159	-0.144
V_s (E|U)	-0.829	-0.368	-0.320	-0.289
V_{ee}^X (U|E)	-0.269	-0.235	-0.209	-0.179

QTAIM also yields properties of interatomic surfaces: values of the surface virial V_s(A|B), *i.e.* the contribution of the A|B surface to the stabilisation of atom A, are also reported in Table 4. These clearly show that the mutual stabilisation of U and O in uranyl is much greater than in S, Se or Te species, and that a slight reduction from S to Te occurs. This data, however, cannot distinguish between stabilisation due to ionic and covalent effects: for this, we turn to the interacting quantum atoms (IQA) approach, and in particular the exchange contribution to the inter-atomic interaction energy V_{ee}^X. This quantity is maximal for E = O, but falls only slightly for S and again for Se and Te. On the surface, these results are at odds with the Wiberg and QTAIM bond order data that indicate greater covalency for the heavier chalcogens. However, it should be noted that these measure subtly different effects: there is greater sharing of electrons in the heavier species, but this is less effective in stabilising the molecular charge distribution, due to the longer bond lengths and

increased orbital energy separation in the heavier complexes. We therefore arrive at a picture of bonding in which covalency increases down the chalcogen group but does not lead to greater stabilisation, while ionicity decreases markedly down the group, thus leading to the much greater overall strength of the U-O bond over those to S, Se and Te, and the relative constancy of the bond strength (as measured by the harmonic force constant) for the latter three species. In this sense, our data suggests that covalency within $[UO_2]^{2+}$ is driven by orbital overlap, increasing the accumulation of density in the internuclear region and strongly stabilising the ion, whereas that within the heavier analogues is more degeneracy-driven. As noted by Tanti et al,[40] the latter form of covalency does not necessarily lead to energetic stabilisation.

As well as the symmetrical ions discussed above, we also examined a mixed analogue of uranyl, $[UOS]^{2+}$, using the same methods. We find U-O bond length of 1.692 Å, slightly longer than in uranyl, and U-S = 2.166 Å, shorter than in $[US_2]^{2+}$. Normal modes at 1113 cm^{-1} and 571 cm^{-1}, and Wiberg bond orders of 2.213 and 2.706 are found for U-O and U-S, reflecting the weakening of the former and strengthening of the latter bond. We interpret these changes as evidence of an inverse trans influence (ITI), in which ligands located *trans*- to electronegative groups are stabilised through a "pushing from below" mechanism on U-centred orbitals. The U-O bond in the asymmetric ion is weaker due to its orientation *trans*- to S, while the U-S bond is stronger as a result of its being *trans*- to O.

Studies of $[UE_2]^{2+}$ cations yield valuable insight into the differences within the chalcogen group, and their high symmetry and small size make calculations tractable, but such bare cations are not experimentally realisable. To examine whether trends noted above are carried through to more realistic systems, we carried out a second set of calculations for complexes with 5 water molecules arranged around the equatorial plane of $[UE_2]^{2+}$. Geometrical and vibrational data (Table 7) are broadly consistent with that for the bare cations[41] and experimental data,[42] with small increases in r(U-E) and decreases in U-E vibrational wavenumbers. Such changes have been noted before[43] and attributed to competition between axial and equatorial ligands for donation into U orbitals. This is also evident in the bond lengths to equatorial water, which get shorter as chalcogen gets heavier. The mixed O/S complex shows further evidence for ITI, in that the U-O bond is longer and weaker and the U-S bond shorter and stronger than in the symmetrical species.

Table 7 Optimised geometry and normal mode vibrations for $[UE_2(H_2O)_5]^{2+}$ (Å and cm^{-1})

	r(U-E)	R(U-OH_2)	ν(symm)	ν(asymm)
O	1.726	2.478	992	1074
S	2.236	2.450	486	499
Se	2.394	2.445	275	349
Te	2.635	2.446	189	266
$[OUS]^{2+}$	1.735 [a] 2.228 [b]	2.462	575 [b]	1017 [a]

[a] U-O; [b] U-S stretch

Table 8 reports selected electronic properties for these $[UE_2(H_2O)_5]^{2+}$ complexes: HOMO-LUMO gaps are rather larger than those found for the bare cations, suggesting equatorial coordination can stabilise these species. NBO charges are markedly smaller than for the bare cations, resulting from further charge transfer from the equatorial ligands into formally empty orbitals on U, to the extent that U in E = Te is predicted to bear a negative charge. Increases in population for 5f, 6d, 7s and 7p orbitals are evident, although in the case of E = S the population of 7p falls to zero when equatorial ligands are present, offset by larger increases in 5f and 6d. Bond critical point properties indicate the same pattern of reduced U-E bond strength resulting from equatorial ligands as noted from bond length and normal mode vibrations. Also apparent is the relative weakness of the equatorial bonds to water, as previously noted for the uranyl ion.[43] Changes in U-E bonds are relatively small compared to the bare cations, such that the patterns of bonding noted for the small models should be transferable to these larger complexes.

Table 8 NBO charge and configuration, bond critical point data and HOMO-LUMO gap for $[UE_2(H_2O)_5]^{2+}$.

	q(U) / e	U configuration /e	ρ^a / au	$\nabla^2\rho$ / au	H / au	HOMO-LUMO / eV
O	+1.705	$7s^{0.17}\,5f^{2.60}\,6d^{1.46}\,7p^{0.30}$	0.352 0.052	+0.361 +0.198	-0.339 -0.003	6.21
S	+0.196	$7s^{0.23}\,5f^{3.03}\,6d^{2.19}\,7p^{0.00}$	0.172 0.055	+0.000 +0.205	-0.110 -0.004	4.30
Se	+0.038	$7s^{0.26}\,5f^{2.99}\,6d^{2.29}\,7p^{0.27}$	0.138 0.056	+0.020 +0.206	-0.078 -0.005	3.81
Te	-0.118	$7s^{0.33}\,5f^{2.92}\,6d^{2.42}\,7p^{0.46}$	0.102 0.056	+0.033 +0.205	-0.048 -0.004	3.16
$[OUS]^{2+}$	+0.102	$7s^{0.20}\,5f^{2.78}\,6d^{1.76}\,7p^{0.37}$	0.335 0.176 0.054	+0.375 -0.009 +0.202	-0.324 -0.114 -0.004	4.68

[a] bcp data is given for U-E bond first, then U-OH_2 bond.

These hydrated models were also used to explore the potential for structural variation in the E = S complex, as the *cis*-uranyl ion has been calculated to be 159 kJ/mol^{-1} higher in energy;[44] this has not been experimentally realised but bending in the uranyl ion has been noted from X-ray structures.[45] A relaxed potential energy scan of the S—U—S angle (Figure 5) revealed a shallow minimum corresponding to a bent arrangement, with an angle of *ca.* 132°. The barrier for relaxation back to the favoured linear orientation is small, such that this geometry may at best be a possible meta-stable state, but we tentatively suggest that bent/non-linear analogues of uranyl may be realisable through suitable choice of ligands. This differs from a previous DFT study on the bare $[US_2]^{2+}$ ion, in which the linear isomer was 171 kJ mol^{-1} higher in energy than a side on η^2-S_2 ligation mode,[24] perhaps indicating the importance of the equatorial ligands. Electronic properties of this bent form are similar to the linear form, but with slightly more positive U (+0.413) stemming from reduced population of valence orbitals on U ($7s^{0.23}\,5f^{2.92}\,6d^{2.09}\,7p^{0.00}$). It is also apparent from Figure 5 that a true *cis*- arrangement of S ligands is not a stable form of this complex, at least according to DFT predictions, with S-U-S = 90° an energy maximum.

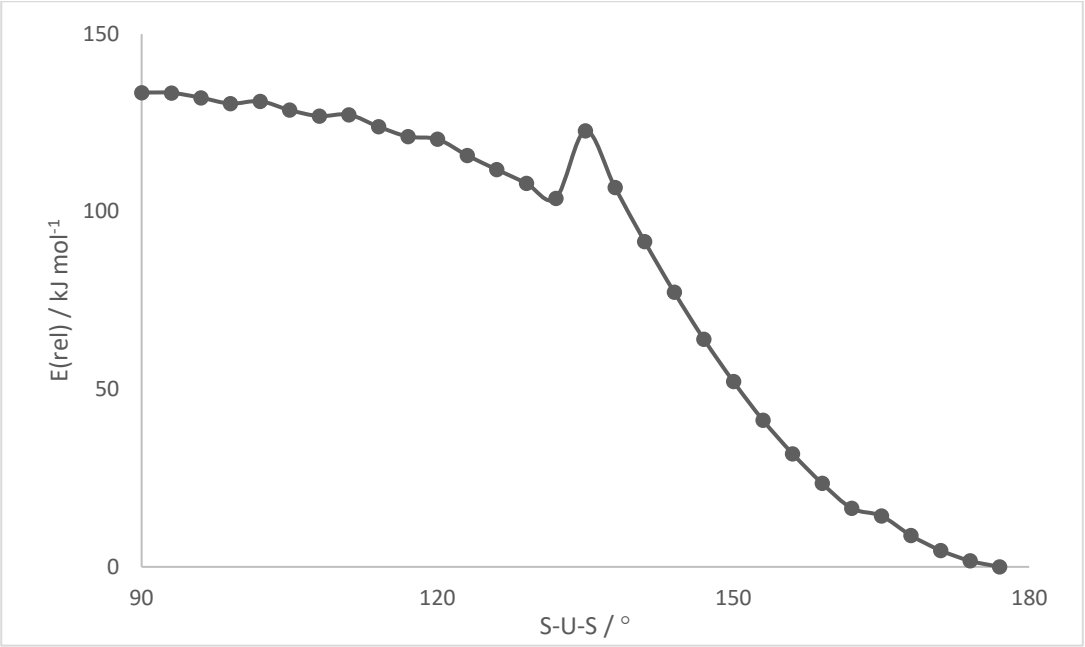

Figure 5 Relative energy of $[US_2(H_2O)_5]^{2+}$ as a function of S—U—S angle.

Changes in the electronic structure as a function of E are reflected in the molecular electrostatic potential that drives molecular recognition through polar interactions such as hydrogen bonding. Figure 6 shows this quantity, mapped onto the 0.001 au isosurface of electron density, for $[UE_2(H_2O)_5]^{2+}$. MEP is positive everywhere due to the net positive charge on the ion, but the trend of most positive values being associated with protons on equatorial waters and least positive with axial E atoms is apparent. Visually, there is little to distinguish such plots, but numerical ranges indicate slightly larger separation of charge for E = O reflecting the greater negative charge on O and increased donation from H_2O into U.

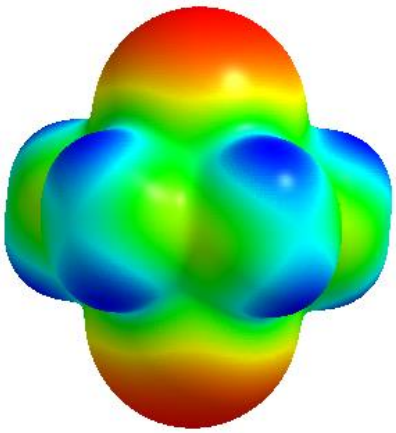	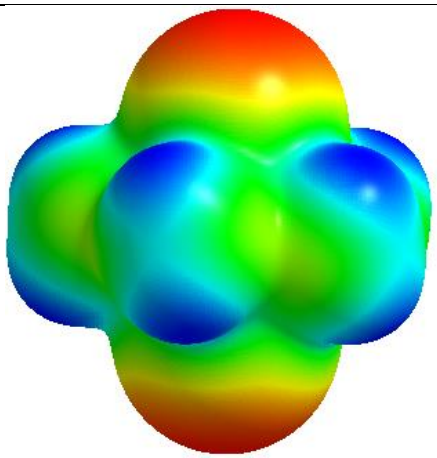	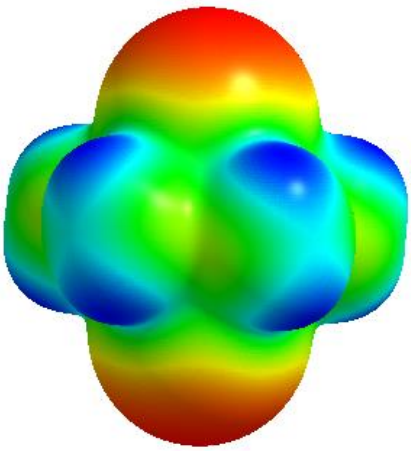
O: +0.2116 to +0.3367 au	S: +0.2198 to +0.3337 au	Se: +0.2190 to +0.3321 au
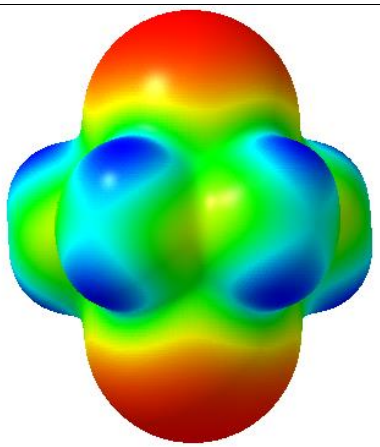	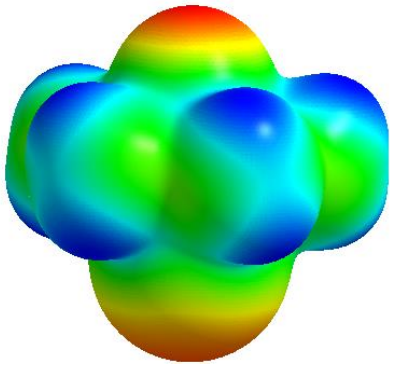	
Te: +0.2192 to +0.3274	OUS: +0.2111 to +0.3351	

Figure 6 Molecular electrostatic potential mapped onto 0.001 au electron density isosurface: colour scheme ranges from red (minimum) to blue (maximum) within ranges shown.

CONCLUSIONS

We have used density functional theory to probe the structure and bonding in analogues of the uranyl cation, replacing O with S, Se and Te. In all cases, linear cations $[UE_2]^{2+}$ are found to be minima on the potential energy hypersurface, confirmed by harmonic frequency calculation. Geometries of these bare cations are broadly as expected, bond lengths increasing steadily down the group. Harmonic frequency data show a more interesting pattern: wavenumbers decrease down the group, but this is largely a consequence of the increased mass of the ligands. Force constants for all stretching and bending modes are large for E = O, and smaller but relatively stable for E = S, Se and Te, suggesting broad similarity of the heavier analogues.

Canonical molecular orbitals are broadly consistent across the series: the HOMO is consistently of σ_u character and the LUMO of φ_u. However, the energy of key valence MOs varies considerably

down the group: all energies increase, but those of occupied ones do more so than virtual, leading to marked closing of the HOMO-LUMO gap from over 6 eV for O to 2.4 eV for Te. Energy separation within occupied orbitals is also reduced, leading to near degeneracy of σ_u and π_u MOs. NBO analysis indicates that the positive charge on U is much larger for E = O than for the heavier complexes, while Wiberg bond order is smallest for E = O and relatively constant for E = S, Se and Te. In all cases, substantial donation from filled orbitals on E into formally empty orbitals on U is evident, with 5*f* and 6*d* orbitals the most populated.

QTAIM analysis often takes the form of using properties of the electron density at the bond critical point. Here though, this data does not accord with the picture obtained from structural or MO data. In particular, bcp properties suggest the U—O bond is stronger and more covalent (large ρ, large negative energy density) than the heavier analogues. This apparent discrepancy can be resolved by consideration of global properties, whether integrated over atomic basins and interatomic surfaces, or plotted along the U—E internuclear vector. This analysis reveals a picture of $[UO_2]^{2+}$ having a qualitatively different electron density distribution from the other complexes, in which the cooperativity of ionic and covalent effects lead to a particularly short bond in which valence shell charge concentrations (VSCCs) of the atoms merge. This in turn means that the electron density does not fall to the low (< 0.1 au) values more commonly seen in metal-ligand bonds. In contrast, the density distribution in $[US_2]^{2+}$ is more typical of metal-ligand bonding.

Combined NBO and QTAIM analysis also yields a more nuanced view of covalency than may be obtained from each technique alone. The atomic orbital make-up of the three bonding U—E NBOs shows a progressive trend of more equal sharing of electrons and reduced energy separation on descending the group, giving rise to increased bond order. However, second-order perturbation analysis identifies the stabilisation due to donation from E to U as being larger for E = O than for heavier analogues due to small orbital energy differences and significant overlap. Stabilisation for E = S is reduced due to reduced overlap, and for E = Se and Te due to increased energy difference. Interacting quantum atom (IQA) data supports this analysis, indicating that stabilisation due to covalency is largest for E = O, despite this having the lowest covalent bond order. This is direct evidence for the concept of energy degeneracy-driven covalency that results in increased sharing of electrons without necessarily yielding greater stabilisation. Explicitly, as the np orbitals on E approach energy degeneracy with the 5f orbitals on U, ΔE_{ML} becomes the more important factor in Equation 1.

Equatorial coordination of water molecules around these cations does not strongly affect the geometric or electronic structure of the core cations, but does stabilise them by increasing HOMO-LUMO gaps and reducing the large positive charge on U. We find some evidence for a meta-stable bent form of $[US_2(H_2O)_5]^{2+}$, albeit with a very small barrier to reversion to the more stable linear form.

REFERENCES

[1] Advanced Inorganic Chemistry, F. A. Cotton, G. Wilkinson, C. A. Murillo and M. Bochmann, 6th Edition. Wiley 1999

[2] R M Diamond, K Street Jr and G T Seaborg, *J. Am. Chem. Soc.*, 1954, **76**, 1461.

[3] Th: A. Avdeef, A. Zalkin, K. N. Raymond and K. O. Hodgson, *Inorg. Chem.*, 1972, **11**, 1083; Pa: J. P. Solar, H. P. G. Burghard, R. H. Banks, A. J. Streitwieser and D. Brown, *Inorg. Chem.*, 1980, **19**, 2186; U: A. J. Streitwieser and U. Müller-Westerhof, *J. Am. Chem. Soc*., 1968, **90**, 7364; Np/Pu: D. G. Karraker, J. A. Stone, E. R. Jones and N. M. Edelstein, *J. Am. Chem. Soc.*, 1970, **92**, 4841.

[4] (a) A. Kerridge, *RSC Adv.*, 2014, **4**, 12078; (b) A. Kerridge and N. Kaltsoyannis. *J. Phys. Chem. A* 2009, **113**, 30, 8737; (c) A. Kerridge, R. Coates and N.Kaltsoyannis, *J. Phys. Chem.* 2009, **113**, 2896.

[5] J. G. Brennan, R. A. Andersen and J. L. Robbins, *J. Am. Chem. Soc*., 1986, **108**, 335.

[6] (a) J. Parry, E. Carmona, S. Coles and M. Hursthouse, *J. Am. Chem. Soc*., 1995, **117**, 2649. (b) M. del Mar Conejo, J. Parry, E. Carmona, M. Schultz, J. G. Brennan, S. M. Beshouri, R. A. Andersen, R. D. Rodgers, S. Coles and M. Hursthouse, *Chem. Eur. J.,* 1999, **5**, 3000.

[7] L. Maron, O. Eisenstein and R. A. Andersen, *Organometallics* 2009**, 28**, 3629.

[8] R. R. Langeslay, G. P. Chen, C. J. Windorff, A. K. Chan, J. W. Ziller, F. Furche and W. J. Evans, *J. Am. Chem. Soc.,* 2017**, 139**, 3387.

[9] N. Kaltsoyannis, P. J. Hay, J. Li, J.-P. Blaudeauand B. E. Bursten, in The Chemistry of the Actinide and Transactinide Elements, 3rd edn. (eds. L. R. Morss, N. Edelstein and J. Fuger) 1893–2012, Springer, Dordrecht, 2006.

[10] See for example E. Lu, S. Sajjad, V. E. J. Berryman, A. J. Wooles, N. Kaltsoyannis and S. T. Liddle, *Nat Commun* 2019, **10,** 634.

[11] (a) A. Kerridge, *Chem. Commun.*, 2017, **53**, 6685; (b) M. L. Neidig, D. L. Clark and R. L. Martin, *Coord. Chem. Rev*., 2012, **257**, 394.

[12] Selected examples: (a) M. Zegke, X. Zhang, I. Pidchenko, J. A. Hlina, R. M. Lord, J. Purkis, G. S. Nichol, N. Magnani, G. Schreckenbach, T. Vitova, J. B. Love and Polly L. Arnold, *Chem. Sci.*, 2019, **10**, 9740; (b) T. Vitova, I. Pidchenko, S. Biswas, G. Beridze, P. W. Dunne, D. Schild, Z. Wang, P. M. Kowalski and R. J. Baker, *Inorg. Chem.,* 2018, **57**, 1735; (c) K. O. Kvashnina, P. M. Kowalski, S. M. Butorin, G. Leinders, J. Pakarinen, R. Bes, H. Li and M. Verwerft, *Chem. Commun.*, 2018, **54**, 9757; (d) T. Vitova, I. Pidchenko, D. Fellhauer, P. S. Bagus, Y. Joly, T. Pruessmann, S. Bahl, E. Gonzalez-Robles, J. Rothe, M. Altmaier, M. A. Denecke and H. Geckeis *Nat. Commun*., 2017, **8**, 16053; (e) S. M. Butorin, A. Modin, J. R. Vegelius, K. O. Kvashnina and D. K. Shuh, *J. Phys. Chem. C*, 2016, **120**, 29397; (f) T. Vitova, J. C. Green, R. G. Denning, M. Loeble, K. Kvashnina, J. J. Kas, K. Jorissen, J. J. Rehr, T. Malcherek and M. A. Denecke, *Inorg. Chem.*, 2015, **54**, 174; (g) K. O. Kvashnina, Y. O. Kvashnin, S. M. Butorin, *J. Electron. Spectrosc.*, 2014, **194**, 27.

[13] Selected examples: (a) E. Epifano, M. Naji, D. Manara, A. C. Scheinost, C. Hennig, J. Lechelle, R. J. M. Konings, C. Guéneau, D. Prieur, T. Vitova, K. Dardenne, J. Rothe and P. M. Martin, *Commun. Chem*., 2019, **2**, 59; (b) S. M. Butorin, K. O. Kvashnina, J. R. Vegelius, D. Meyer and D. K. Shuh, *Proc. Nat. Acad. Sci.* 2016, **113**, 8093; (c) S. M. Butorin, K. O. Kvashnina, A. L. Smith, K. Popa and P. M. Martin, *Chem. Eur. J.*, 2016, **22**, 9693; (d) A. Walshe, T. Prußmann, T. Vitova and R. J. Baker, *Dalton. Trans.*, 2014, **43**, 4400;

[14] E. I. Solomon, B. Hedman, K. Hodgson, A. Dey and R. K. Szilagyi, *Coord. Chem. Rev.*, 2005, **249**, 97.

[15] (a) J. Su, E. R. Batista, K. S. Boland, S. E. Bone, J. A. Bradley, S. K. Cary, D. L. Clark, S. D. Conradson, A. S. Ditter, N. Kaltsoyannis, J. M. Keith, A. Kerridge, S. A. Kozimor, M. W. Loble, R. L. Martin, S. G. Minasian, V. Mocko, H. S. La Pierre, G. T. Seidler, D. K. Shuh, M. P. Wilkerson, L. E. Wolfsberg and P. Yang, *J. Am, Chem. Soc.*, 2018, **140**, 17977; (b) J. N. Cross, J. Su, E. R. Batista, S. K. Cary, W. J. Evans, S. A. Kozimor, V. Mocko, B. L. Scott, B. W. Stein, C. J. Windorff, P. Yang, *J. Amer. Chem. Soc.*, 2017, **139**, 8667; (c) S. G. Minasian, J. M. Keith, E. R. Batista, K. S. Boland, D. L. Clark, S. A. Kozimor, R. L. Martin, D. K. Shuh and T. Tyliszczak, *Chem. Sci.*, 2014, 5, 351; (d) L. P. Spencer, P. Yang, S. G. Minasian, R. E. Jilek, E. R. Batista, K. S. Boland, J. M. Boncella, S. D. Conradson, D. L. Clark, T. W. Hayton, S. A. Kozimor, R. L. Martin, M. M. MacInnes, A. C. Olson, B. L. Scott, D. K. Shuh and M. P Wilkerson, *J. Amer. Chem. Soc.*, 2013, **135**, 2279; (e) S. G. Minasian, J. M. Keith, E. R. Batista, K. S. Boland, D. L. Clark, S. D. Conradson, S. A. Kozimor, R. L. Martin, D. E. Schwarz, D. K. Shuh, G. L. Wagner, M. P. Wilkerson, L. E. Wolfsberg and P. Yang, *J. Amer. Chem. Soc.*, 2012, **134**, 5586; (f) S. A. Kozimor,

P. Yang, E. R. Batista, K. S. Boland, C. J. Burns, D. L. Clark, S. D. Conradson, R. L. Martin, M. P. Wilkerson and L. E. Wolfsberg, *J. Amer. Chem. Soc.*, 2009, **131**, 12125.

[16] N. Kaltsoyannis, *Chem. Eur. J.*, 2018, **24**, 2815.

[17] N. Kaltsoyannis, *Inorg. Chem.*, 2013, **52**, 3407.

[18] R. J. Baker, *Chem. Eur. J.*, 2012, **18**, 16258

[19] E. O'Grady and N. Kaltsoyannis, *J. Chem. Soc., Dalton Trans*., 2002, 1233.

[20] R. G. Denning, *J. Phys. Chem. A*, 2007, **111**, 4125.

[21] P. S.Bagus H. Freund, H. Kuhlenbeck and E. S.Ilton, *Chem Phys Lett*., 2008, **455**, 331.

[22] (a) I. Fryer-Kanssen and A. Kerridge, *Chem Comm*., 2018, **54**, 9761; (b) H. S. La Pierre and K. Meyer, *Inorg. Chem.*, 2013, **52**, 529.

[23] C. Fillaux, D. Guillaumont, J.-C. Berthet, R. Copping, D. K. Shuh, T. Tyliszczak and C. Den Auwer, *Phys. Chem. Chem. Phys.*, 2010, **12**, 14253.

[24] C. C. L. Pereira, M. del Carmen Michelini, J. Marçalo, Y. Gong and J. K. Gibson, *Inorg. Chem.*, 2013, **52**, 14162.

[25] J. L. Brown, S. Fortier, G. Wu, N. Kaltsoyannis and T. W. Hayton, *J. Am. Chem. Soc*., 2013, **135**, 5352.

[26] D. P. Mills, O. J. Cooper, F. Tuna, E. J. L. McInnes, E. S. Davies, J. McMaster, F. M. Oro, W. Lewis, A. J. Blake and S. T. Liddle, *J. Am. Chem. Soc*., 2012, **134**, 10047.

[27] A. F. Lucena, N. A. G. Bandeira, C. C. L. Pereira, J. K. Gibson, J Marçalo, *Phys. Chem. Chem. Phys*., 2017,**19**, 10685.

[28] (a) J. P. Perdew, K. Burke and M. Ernzerhof, *Phys. Rev. Lett.*, 1996, **77**, 3865; (b) C. Adamo and V. Barone, *J. Chem. Phys.*, 1999, **110**, 6158.

[29] F. Weigend and R. Ahlrichs, *Phys. Chem. Chem. Phys*., 2005, **7**, 3297.

[30] W. Küchle, M. Dolg, H. Stoll and H. Preuss, *J. Chem. Phys.*, 1994, **100**, 7535.

[31] M. J. Frisch, G. W. Trucks, H. B. Schlegel, G. E. Scuseria, M. A. Robb, J. R. Cheeseman, G. Scalmani, V. Barone, G. A. Petersson, H. Nakatsuji, X. Li, M. Caricato, A. Marenich, J. Bloino, B. G. Janesko, R. Gomperts, B. Mennucci, H. P. Hratchian, J. V. Ortiz, A. F. Izmaylov, J. L. Sonnenberg, D. Williams-Young, F. Ding, F. Lipparini, F. Egidi, J. Goings, B. Peng, A. Petrone, T. Henderson, D. Ranasinghe, V. G. Zakrzewski, J. Gao, N. Rega, G. Zheng, W. Liang, M. Hada, M. Ehara, K. Toyota, R. Fukuda, J. Hasegawa, M. Ishida, T. Nakajima, Y. Honda, O. Kitao, H. Nakai, T. Vreven, K. Throssell, J. A. Montgomery, Jr., J. E. Peralta, F. Ogliaro, M. Bearpark, J. J. Heyd, E. Brothers, K. N. Kudin, V. N. Staroverov, T. Keith, R. Kobayashi, J. Normand, K. Raghavachari, A. Rendell, J. C. Burant, S. S. Iyengar, J. Tomasi, M. Cossi, J. M. Millam, M. Klene, C. Adamo, R.

Cammi, J. W. Ochterski, R. L. Martin, K. Morokuma, O. Farkas, J. B. Foresman, and D. J. Fox, Gaussian09 Revision D.01, Gaussian Inc., Wallingford CT, 2009.

[32] A. E. Reed, L. A. Curtiss and F. Weinhold, *Chem. Rev*., 1988, **88**, 899.

[33] R. F. W. Bader, Atoms in molecules: a quantum theory, Clarendon Press ; OUP, Oxford 1994.

[34] T. A. Keith, AIMAll, TK Gristmill Software, Overland Park KS, USA, 2017.

[35] M. A. Blanco, A. Martín Pendás, and E. Francisco *J. Chem. Theory Comput*., 2005, **1**, 1096. Data taken from Hartree-Fock calculations due to complications arising from use of IQA on Kohn-Sham orbitals.

[36] S. Alvarez, *Dalton Trans.*, 2013, 42, 8617.

[37] Analogous data for uranyl has been reported, values here are in general agreement with minor differences due to different basis set employed: V. Vallet, U. Wahlgren and I. Grenthe, *J. Phys. Chem. A*, 2012, **116**, 12373.

[38] A. Kerridge, *Chem. Commun*., 2017, **53**, 6685.

[39] G. Eickerling and M. Reiher, *J. Chem. Theory Comput*., 2008, **4**, 286.

[40] J. Tanti, M. Lincoln A. Kerridge, *Inorganics* 2018, **6**, 88.

[41] See for example: (a) A. E. Clark, A. Samuels, K. Wisuri, S. Landstrom and T. Saul, *Inorg. Chem.* 2015**, 54**, 6216; (b) S. Kerisit and C. Liu, *J.Phys. Chem. A* 2013**, 117,** 6421; (c) K. E. Gutowski and D. A. Dixon, *J. Phys. Chem. A* 2006, **110**, 8840; (d) V. Vallet, U. Wahlgren, B. Schimmelpfennig, Z. Szabó, I. Grenthe *J. Am. Chem. Soc.* 2001, **123**, 11999.

[42] K. E. Knope and L. Soderholm, *Chem Rev*., 2013, **113**, 944.

[43] P. Di Pietro and A. Kerridge, *Inorg. Chem.*, 2016, **55**, 573.

[44] G. Schreckenbach, P.J. Hay and R.L. Martin, *Inorg. Chem.*, 1998, **37**, 4442.

[45] For a review see T. W. Hayton, *Dalton Trans.*, 2018, **47**, 1003.